Soft-graphoepitaxy using nanoimprinted polyhedral oligomeric silsesquioxane substrates for the directed self-assembly of PS-b-PDMS

Dipu Borah, Claudia Simao, Ramsankar Senthamaraikannan, Sozaraj Rasappa, Achille Francone, Olivier Lorret, Mathieu Salaun, Barbara Kosmala, Nikolaos Kehagias, Marc Zelsmann, et al.

Soft-graphoepitaxy using nanoimprinted polyhedral oligomeric silsesquioxane substrates for the directed self-assembly of PS-*b*-PDMS

Dipu Borah [a,b,c], Claudia D. Simao [d], Ramsankar Senthamaraikannan [a,c], Sozaraj Rasappa [a,b,c], Achille Francone [d], Olivier Lorret [e], Mathieu Salaun [f], Barbara Kosmala [a,b], Nikolaos Kehagias [d], Marc Zelsmann [f], Clivia M. Sotomayor-Torres [d,g], Michael A. Morris [a,b,c,*]

[a] *Department of Chemistry, University College Cork, Cork, Ireland*
[b] *Tyndall National Institute, Lee Maltings, Prospect Row, Cork, Ireland*
[c] *Centre for Research on Adaptive Nanostructures and Nanodevices (CRANN), Trinity College Dublin, Dublin 2, Ireland*
[d] *Catalan Institute of Nanotechnology, Campus de Bellaterra, Edifici CM3, ES 08193 Bellaterra, Barcelona, Spain*
[e] *Profactor GmbH, Functional Surfaces and Nanostructures, 4407 Steyr-Gleink, Austria*
[f] *Laboratoire des Technologies de la Microélectronique, CNRS/UJF-Grenoble1/CEA LTM, 17 rue des Martyrs, 38054 Grenoble, France*
[g] *Catalan Institution for Research and Advanced Studies, ICREA, 08010 Barcelona, Spain*

We report here the fabrication of periodic sub-25 nm diameter size cylinder structures using block copolymer (BCP) directed self-assembly on nanoimprinted topographically patterned substrates. Tailored polyhedral oligomeric silsesquioxanes (POSSs) films were spin coated onto silicon substrates and were patterned by nanoimprint lithography to pro-duce topographies commensurable with the BCP domain spacing. The chemistry of the POSS was tuned to control the alignment and orientation of the BCP films. The substrates were used to direct the microphase separation (following toluene solvent annealing) of a hexagonal structure forming polystyrene-*block*-polydimethylsiloxane (PS-*b*-PDMS) having a domain spacing of 42.6 nm and PDMS cylinder widths of 23.7 nm. On more hydrophilic POSS substrates the cylinders were obtained parallel to the substrate plane and aligned with the topography. In contrast, in more hydrophobic POSS patterns, the cylinders align perpendicular to the substrate plane. The use of these methods for the nanofabrication of vias, nanofluidic devices or interconnect structures of sub-25 nm feature size is discussed.

1. Introduction

The increasing performance of semiconductor electronics has been coupled to the improved resolution of the lithographic process and the dimensions of critical circuit elements are shrinking below 10 nm. The continued development of nanotechnology is reliant on the fabrication of periodic arrays of nanosized structures with very high precision. The most sophisticated semiconductor devices, such as microprocessors and memory chips, are patterned with multi-level projection UV lithography [1] but methods such as thermal [2], e-beam [3,4], and X-ray [5] lithography can also facilitate patterns of feature size around 10 nm. In parallel to these 'top-down' engineering approaches, 'bottom-up' techniques based on the hierarchical self-assembly of molecular building blocks through molecular recognition and molecule-surface interactions are being explored [6]. There are advantages and drawbacks

* Corresponding author at: Department of Chemistry, University College Cork, Cork, Ireland. Tel.: +353 214902180; fax: +353 214274097.
E-mail address: m.morris@ucc.ie (M.A. Morris).

Table 1
Details of polymer brush and block copolymer characteristics.

Molecular weight, (M_n), (g/mol)	Polydispersityindex, M_w/M_n	Mole fraction of PS, (%)	Volume fraction of PDMS, ϕ_{PDMS}	Description of polymer
5000	1.07	–	–	Hydroxyl-terminated PDMS
45,500	1.15	0.60	0.34	Cylindrical PS-*b*-PDMS

M_n: number average molecular weight, M_w: weight average molecular weight, and ϕ: volume fraction.

in both approaches. In top-down methodologies further downsizing is critically related to issues such as diffraction limit of optical lithography, thermal management and resist/mask integrity. On the other hand, it is highly challenging to achieve long-range translational order and physical robustness of the self-assembled structures to facilitate pattern transfer to the substrate [7–9].

Directed self-assembly (DSA) – a promising technique where the alignment (i.e. relative to a surface direction or feature) is guided by an external field, chemistry or topography can help in the precise positioning self-assembling materials. Nanoimprint lithography (NIL) combined with block copolymer (BCP) microphase separation may provide a complementary method to produce precise arrangements of structures at substrates [10–12]. NIL is a soft lithography tool that permits replication of a ultrasmall, patterned stamp in a polymer thin film [13]. Nanoimprinting a BCP film can guide the self-assembly of the pattern allowing control of alignment and orientation (direction to the surface plane). This soft lithography technique was first reported by Li and Huck on polystyrene-*block*-polymethylmetacrylate (PS-*b*-PMMA) [14]. Many studies have been devoted to PS-*b*-PMMA since it is compatible with established microelectronic fabrication [15–17]. These studies have shown that lamellar or cylindrical BCP structures could be obtained on surfaces with domain spacings (pitches) varying from 35 to 50 nm. However, the PS-*b*-PMMA system has a relatively low Flory–Huggins parameter which limits the lowest domain spacing that can be attained. Other BCPs capable of smaller dimensions such as polystyrene-*block*-polyethyleneoxide (PS-*b*-PEO), with a lamellar structure of 25 nm pitch [18] and polystyrene-*block*-polyactide (PS-*b*-PLA) with 20 nm pore diameter cylinder structures [19] have been reported. However, one of the most exciting systems is the polystyrene-*block*-polydimethylsiloxane (PS-*b*-PDMS) BCP with sub-10 nm feature sizes reported recently by Park et al., employing NIL-assisted DSA [20]. This BCP is very promising since its Flory–Huggins parameter ($\chi = 68/T - 0.037$) is relatively high and regular self-assembly can be readily achieved [21]. In the PS-*b*-PDMS system two major challenges arise: strong dewetting from surface due to the high hydrophobicity and surface energy of the PDMS component as well as the difficulty of controlling feature orientation. To overcome these limitations, a surface pretreatment with a PDMS brush has usually been employed [22,23] and these results in good surface coverage and controlled parallel orientation of features [24–26]. However, the perpendicular orientation of the BCP cylinders is also of interest e.g. *via* fabrication but results to date suggest that this phase as metastable and usually degenerates into the more stable parallel alignment [16]. Silicon containing polymers such as polyhedral oligomeric silsesquioxanes (POSSs) might allow controlled tuning of the substrate and in the present work; three POSS derivatives with different surface energy were employed and topographically patterned by UV-NIL. These substrates were used to direct the self-assembly of PS-*b*-PDMS. The results show that this combined patterning methodology and the use of carefully designed materials might have significant impact on large-area, inexpensive nanofabrication.

2. Materials and methods

2.1. Materials

OctaSilane POSS® (POSS), Acrylo POSS® (POSS-acrylo) and Epoxy POSS® (POSS-epoxy) were purchased from Hybrid Plastics. 1,2-epoxy-5-hexene, styrene, platinum(0)-1,3-divinyl-1,1,3,3 tetramethyldisiloxane complex solution (Karstedt's catalyst), toluene and ethyl-L-lactate were purchased from Sigma-Aldrich. The photoinitiators Irgacure®

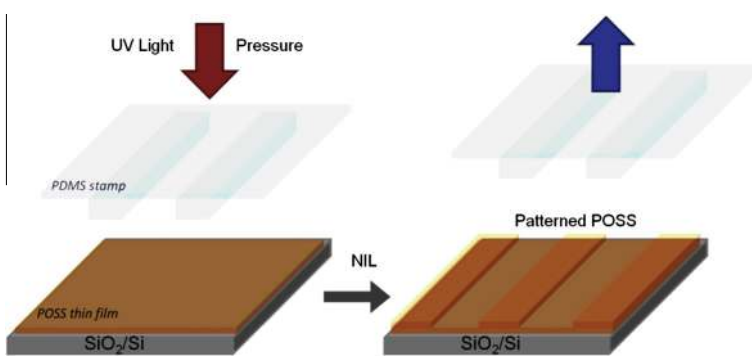

Scheme 1. Schematic of fabrication of patterned POSS substrates by UV-NIL.

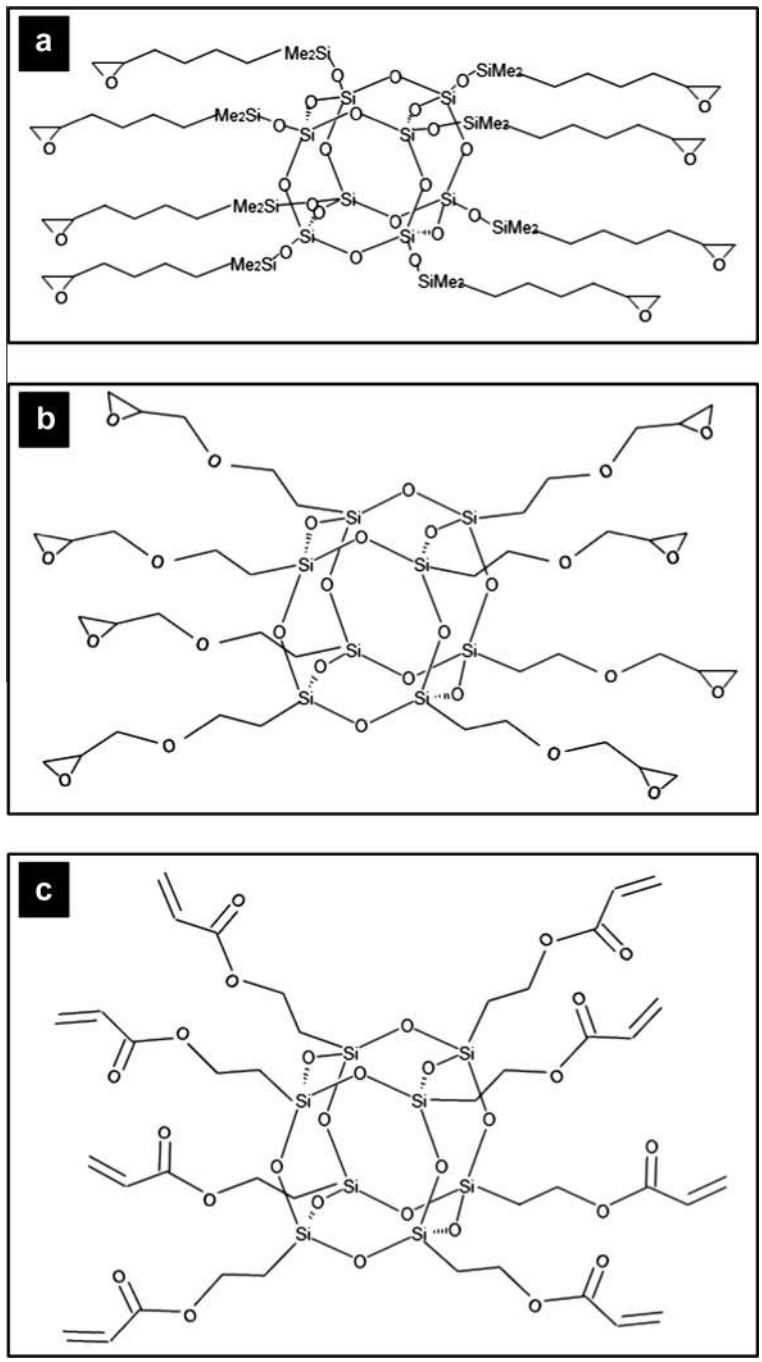

Scheme 2. Structural formulae of POSS derivatives: POSS-C6 (a), POSS-epoxy (b) and POSS-acrylo (c).

250 (iodonium (4-methylphenyl) [4-(2-methylpropyl)phenyl]-hexafluorophosphonate, 75 wt% in propylene carbonate), Irgacure® 819 (Bis(2,4,6 trimethylbenzoyl)-phenylphosphineoxide) and the sensitizer Genocure® ITX (isopropyl thioxanthone) were generously provided by respectively BASF Resins and RAHN AG Energy Curing. A hydroxyl-terminated polydimethylsiloxane (PDMS) homopolymer and a cylinder-forming PS-*b*-PDMS diblock copolymer were purchased from Polymer Source, Inc., Canada, and used as received. Detail characteristics of the polymers are summarized in Table 1. Toluene (99.8%, anhydrous), sulphuric acid (98%) and hydrogen peroxide (30%) were purchased from Sigma–Aldrich and used without further purification unless otherwise stated. De-ionized water was used wherever necessary. Planar substrates used were polished test grade reclaimed 8"

Table 2
Patterned POSSs wettability characteristics.

POSS type	Contact angle (CA) (°)	Surface free energy (SFE) (mN/m)
POSS-epoxy	72	42
POSS-acrylo	62	43
POSS-C6	84	30

Table 3
Patterned POSSs elemental composition characterization.

POSS type	XPS spectral line (eV)				
	Si 2p	Si 2s	C 1s	O 1s	O KILL
POSS-epoxy	103.50	54.30	285.71	533.07	980.07
POSS-acrylo	103.18	154.10	285.71	533.07	979.28
POSS-C6	102.27	153.53	284.29	533.07	979.28

silicon ⟨100⟩ wafers (B doped, *p*-type, thickness 650 μm, and resistivity 6–14 ohm cm) with a native oxide layer of few nanometers (~2 nm). No attempt was taken to remove the native oxide of a few nanometer depths.

2.2. Functionalized POSS-C6 synthesis

OctaSilane POSS cages bearing eight dimethylsilyloxy groups were functionalized by a hydrosilylation reaction carried out on the Si–H functions. Typically, 2 g (1.96 mmol) of OctaSilane POSS were dissolved in 10 mL of anhydrous toluene. 1.96∗8 mmol (8 ligands) of 1,2-epoxy-5-hexene (+10% excess) were added to the mixture with 10 drops of Karstedt's catalyst. The reaction was carried out at 80 °C during 4 h under an argon flow. Solvent, catalyst and material that did not react were then evaporated under reduced pressure on a rotary evaporator. A clear brown solution of epoxy monomer was obtained.

The POSS resists were prepared by dissolving 25 g of POSS monomer in 75 mL ethyl-L-lactate. 2 mol% (relative to epoxy groups) of Irgacure® 250 (photoinitiator absorving in the interval 275–325 nm in wavelength) conjugated with 0.5 wt% of Genocure® ITX (sensitizer absorbing in the interval 340–400 nm) or 2 mol% (relative to acrylate groups) of Irgacure® 250 (photoinitiator absorving in the interval 275–370 nm in wavelength) were added to the solution in order to allow UV polymerization of the resist during the UV-NIL process.

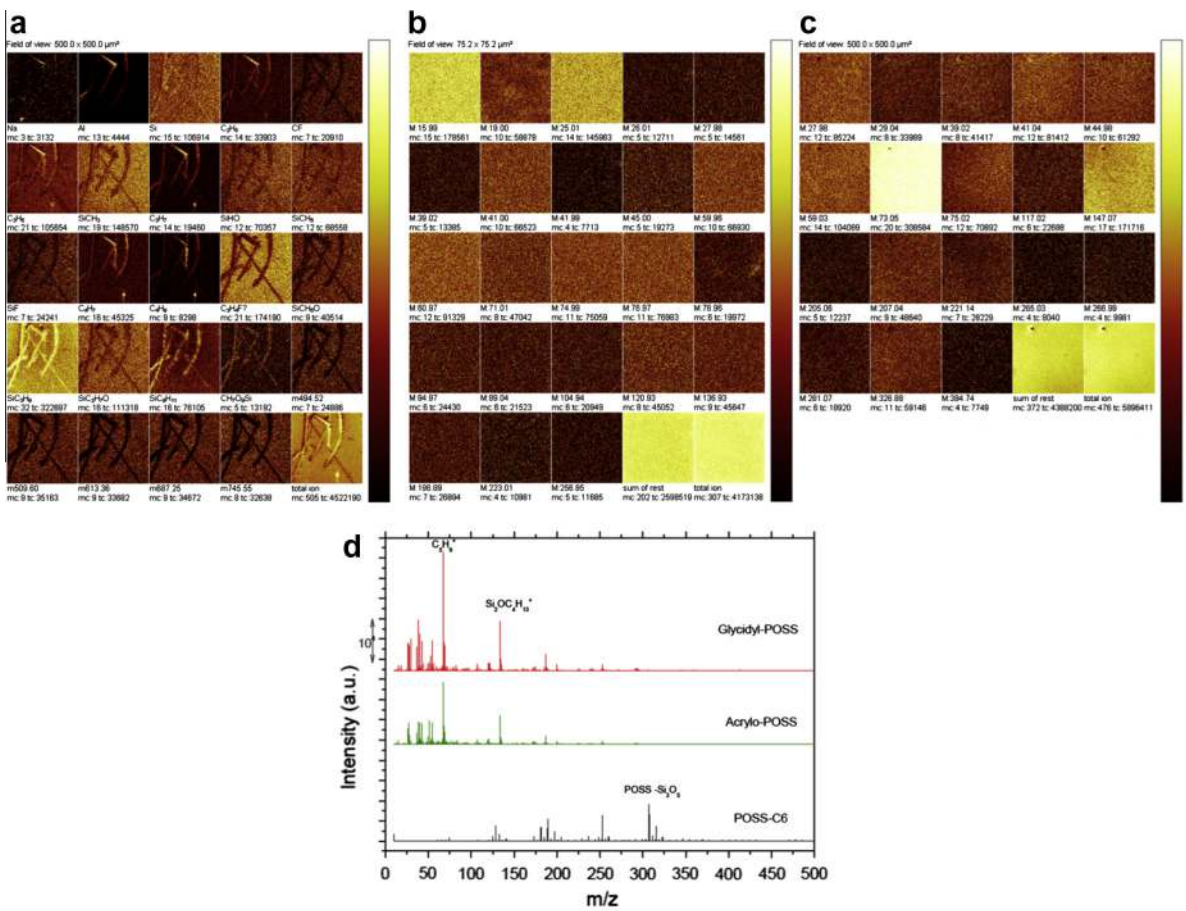

Fig. 1. ToF-SIMS analysis for POSS-C6 (a), POSS-epoxy (b) and POSS-acrylo (c), and related full spectra (d) showing the characteristic POSS peaks and homogeneity of surface composition.

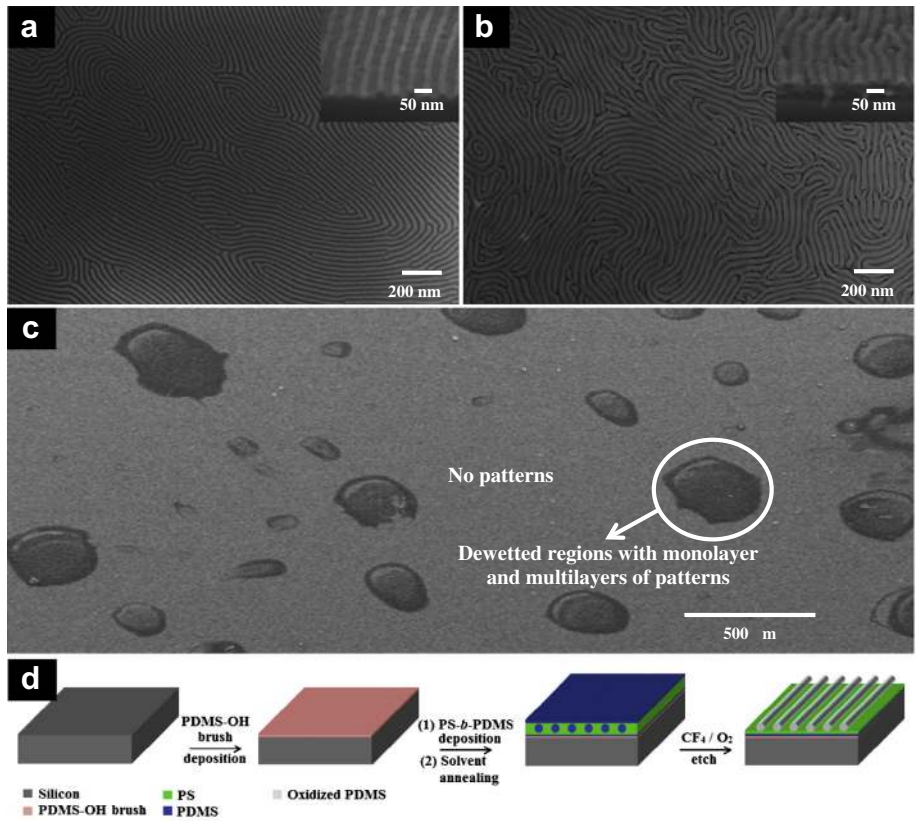

Fig. 2. Top-down SEM images of *in-plane* PDMS cylinders after sequential CF_4 and O_2 plasma etches of microphase separated PS-*b*-PDMS film on PDMS-OH brush anchored silicon substrate with (a) monolayer, and (b) multilayers of PDMS cylinders. Insets, (a and b) are the cross-section SEM images of *in-plane* PDMS cylinders showing monolayer and multiple layers of PDMS cylinders. Low magnification SEM image in (c) shows poor coverage and dewetting issue with PDMS-OH brush. Schematic of self-assembled PS-*b*-PDMS film on planar substrate anchored with a PDMS-OH brush and sequential etching processes is presented in (d).

2.3. Fabrication of nanopatterned POSS thin films by nanoimprint lithography

Nanopatterns on POSS substrates were fabricated by a soft UV assisted-nanoimprint lithography (UV-NIL) technique and the schematic details are given in Scheme 1. Molds were first treated with an anti-sticking layer (Optool DSX, Daikin Chemicals) based on fluorosilanes. This layer has a thickness of about 3 nm and results in a surface free energy of 10.5 mN m^{-1} and allows even demolding after imprint. The silicon molds were reproduced in PDMS pouring a PDMS prepolymer mixture over the silicon mold and curing it at 80 °C for 3 h, in an oven. POSS thin films were imprinted by UV-NIL, bringing a PDMS stamp in contact to the POSS film applying a 2 bar pressure for 5 min while exposing to UV light.

2.4. Deposition of PDMS-OH brush

Silicon substrates were cleaned in a piranha solution (1:3 v/v 30% H_2O_2:H_2SO_4) at 90 °C for 60 min, rinsed with deionized water (resistivity $\geqslant$ 18 MΩ cm^{-1}) several times, and were blown dry with N_2. Piranha activation removes any organic contaminant, greases and creates hydroxyl groups on the silicon substrates. A hydroxyl-terminated polymer brush solution of 1.0 wt% in toluene was prepared by dissolving the appropriate amount of the polymer. The brush solution was spin-coated onto the substrates at 3000 rpm for 30 s. Samples were annealed in a vacuum oven (Townson & Mercer EV018) at 170 °C under vacuum (−1 bar) for 6 h. This allows the end-functional hydroxyl groups of the brush to condense with surface silanol groups and anchor the brushes to the substrate. Unbound polymers were removed by sonication (Cole-Palmer 8891 sonicator) and rinsing in toluene.

2.5. Deposition of PS-b-PDMS and thin film preparation

Thin films of PS-*b*-PDMS were prepared by depositing a dilute solution (1.0 wt%) of the diblock copolymer in toluene onto polymer brush modified planar and NIL POSS silicon substrates by spin coating (3200 rpm and 30 s). As-cast thin films were solvent annealed in glass jars under saturated toluene environment at room temperature (∼15 °C) for 3 h. Samples were removed from the glass jars after the desired anneal time and allowed to evaporate the trapped solvent at ambient conditions.

2.6. Plasma etch processes

Following, BCP film formation, atomic force microscopy cannot readily show the microphase separated structure

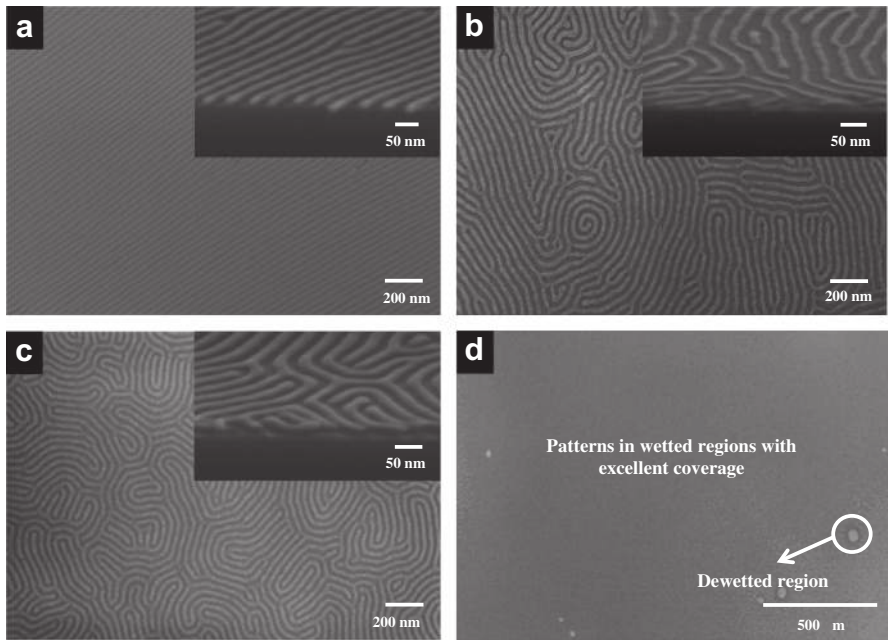

Fig. 3. Top-down SEM images of *in-plane* PDMS cylinders after sequential CF_4 and O_2 plasma etches of microphase separated PS-*b*-PDMS film on planar (a) POSS-C6, (b) POSS-epoxy, and (c) POSS-acrylo deposited silicon substrates. Insets, (a–c) are the cross-section SEM images of *in-plane* PDMS cylinders showing monolayer of PDMS cylinders. Low magnification SEM image in (d) shows excellent coverage with minor dewetting issue in POSS-C6 and found to be similar in POSS-epoxy and POSS-acrylo.

because of the presence of a homogeneous surface wetting layer of PDMS which must be removed to reveal the BCP arrangement [27]. The solvent annealed PS-*b*-PDMS films were first treated with a CF_4 (15 sccm) plasma for 5 s to remove any surface PDMS layer followed by an O_2 (30 sccm) plasma for 10 s with an ICP and RIE powers of 1200 W and 30 W, respectively, at 15 mT with Helium backside cooling pressure of 5 T. These steps follow similar methodology developed by Ross and Jung [27]. The process removes the PS component and forms an oxidized form of PDMS on the substrate. The sequential etching process was accomplished in an OIPT Plasmalab System100 ICP180 etch tool.

2.7. Material analysis

^{1}H NMR and ^{13}C NMR spectra were recorded on a 300 MHz Bruker (B-ACS 60) NMR spectrometer in deuterated chloroform ($CDCl_3$). Infrared spectra were performed on a Bruker Tensor 37 spectrometer. Contact angles and surface free energy measurements were carried out using a Krüss DSA 100 goniometer. Contact angles were measured by the static sessile drop method. Surface free energy was calculated from the measured contact angles of deionized water, diiodomethane and ethylene glycol using the Owens–Wendt model [28]. Film thickness was determined by ellipsometry (Plasmos SD2000 Ellipsometer). An average of three readings collected from different locations on a sample surface was reported as the film thickness result.

The NIL POSS and BCP on NIL POSS surfaces were characterized by contact angle, surface free energy, time-of-flight secondary ion mass spectrometry (ToF-SIMS), X-ray photoelectron spectroscopy (XPS) and field emission scanning electron microscopy (FE-SEM) as well as energy dispersive X-ray analysis (EDX). To measure the surface free energy, a 2 μL drop of de-ionized water was measured using a Oca 15+ Plus, from Dataphysics and the images processed with SCA20 software. Top-down and cross-sectional SEM images of samples were obtained by a high resolution (<1 nm) Field Emission Zeiss Ultra Plus-Scanning Electron Microscope with a Gemini® column operating at an accelerating voltage of 5 kV. The profile images of the surfaces were used to measure the film thickness. For ToF-SIMS analysis, a ToF-SIMS IV (ION-TOF) spectrometre was used. The ion beam was a 25 keV Bi^{3+} source (15 ns pulses). Secondary ions were accelerated to 2 keV and the mass analyzed by time of flight and post-accelerated to 10 keV after detection. The abundance of the ions detected was normalized to the total ion abundance. Finally, the XPS experiments were performed in a PHI 5500 Multitechnique System (from Physical Electronics) with a monochromatic X-ray source (Al Kα radiation). Binding energies were calibrated using a 3d5/2 Ag line. The pass energy used was 187.5 eV for survey spectra and 23.5 eV for individual photoelectron peaks.

3. Results and discussion

3.1. Synthesis and characterization of POSS-C6

The epoxy-functionalized POSS monomer POSS-C6 was prepared according to a protocol published by Crivello and Malik [29]. The infrared spectra of POSS-C6 shows the

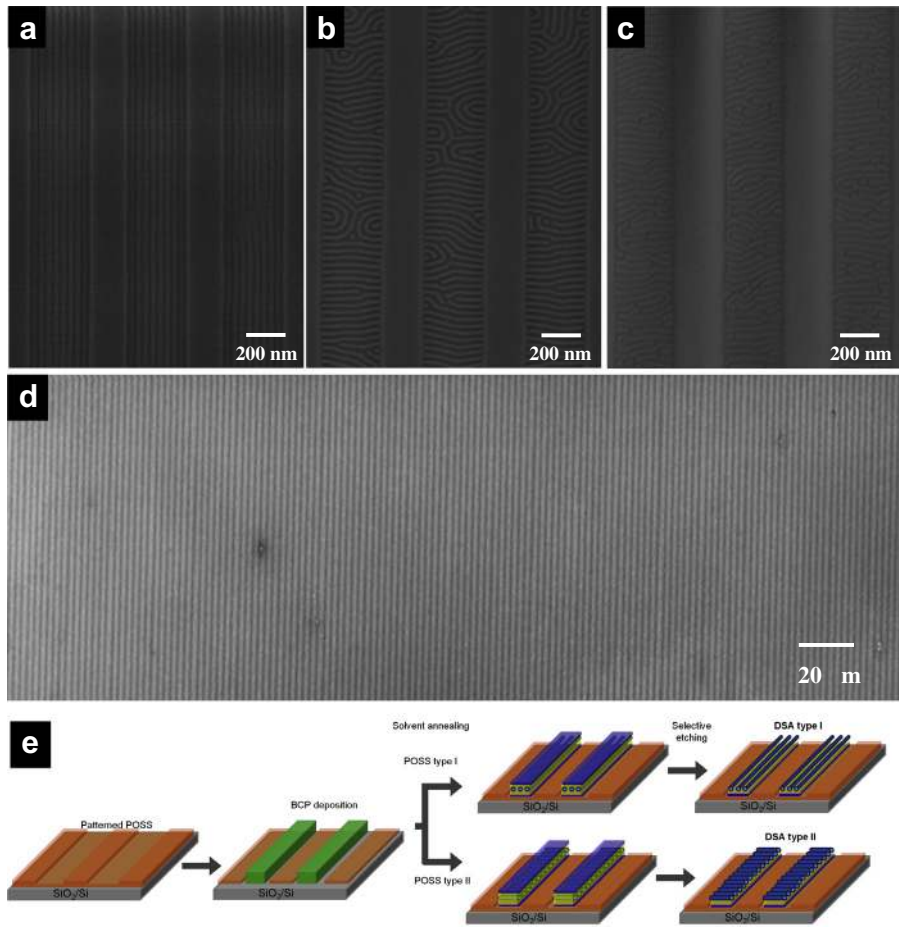

Fig. 4. Top-down SEM images of *in-plane* PDMS cylinders after sequential CF_4 and O_2 plasma etches of microphase separated PS-*b*-PDMS film on patterned (a) POSS-C6, (b) POSS-epoxy, and (c) POSS-acrylo deposited silicon substrates. Low magnification SEM image in (d) shows excellent coverage of the BCP after microphase separation on POSS-C6. Schematic of controlling orientation of features as a function of POSS hydrophilicity is shown in (e).

characteristic POSS cage Si–O–Si peak at 1100 cm^{-1} which is largely unchanged after hydrosilylation suggesting that the structure survives the processing. In addition to the strong stretching bands of the aliphatic C–H bonds at 2900 cm^{-1}, a small band is present at 3055 cm^{-1} corresponding to the C–H band in the epoxy ring. The complete functionalization of the POSS cages occurs after 4 h and can be evidenced spectroscopically by the disappearance of the signals related to the Si–H bond: at 2140 cm^{-1} and at 4.2 ppm in the IR and ^1H NMR spectra, respectively (see Supporting Information). The other two derivatives, the POSS-epoxy and the POSS-acrylo were available commercially. Structural formulae of the three POSS derivatives are given in Scheme 2.

3.2. Patterned POSS characterization

Patterned POSS substrates have three purposes: (a) tuning the surface chemistry to facilitate good surface wetting of the BCP, (b) defining BCP pattern orientation and (c) defining pattern alignment by graphoepitaxy. The characterization of the samples POSS-C6, POSS-epoxy and POSS-acrylo are summarized in Table 2. The surface free energies of POSS-epoxy and POSS-acrylo are similar whilst that of POSS-C6 is markedly different. POSS surfaces were further characterized by XPS (*spectra omitted for the sake of brevity*). The results of the three POSS surfaces are resumed in Table 3 and show the expected element composition in Si, O and C. The silicon 2p binding energies are consistent with more hydrophilic substrates having higher electro-deficiency for this element.

The ToF-SIMS analysis of the three samples evidence the characteristic POSS peaks in the low mass region as detailed in Fig. 1. The difference between POSS-C6 and the other two is that there is a $Si(CH_3)_2$ $m/z = 59$ between the cage structure and the ligand. ToF-SIMS images showed high homogeneity of the surface composition. The thickness of the residual layer in all samples varied between 20 and 50 nm, as measured by FE-SEM profile images.

3.3. Effect of PDMS-OH brush on BCP self-assembly

PDMS-OH brushes are generally used in the preparation of films of this BCP [27,30,31]. The PDMS brush

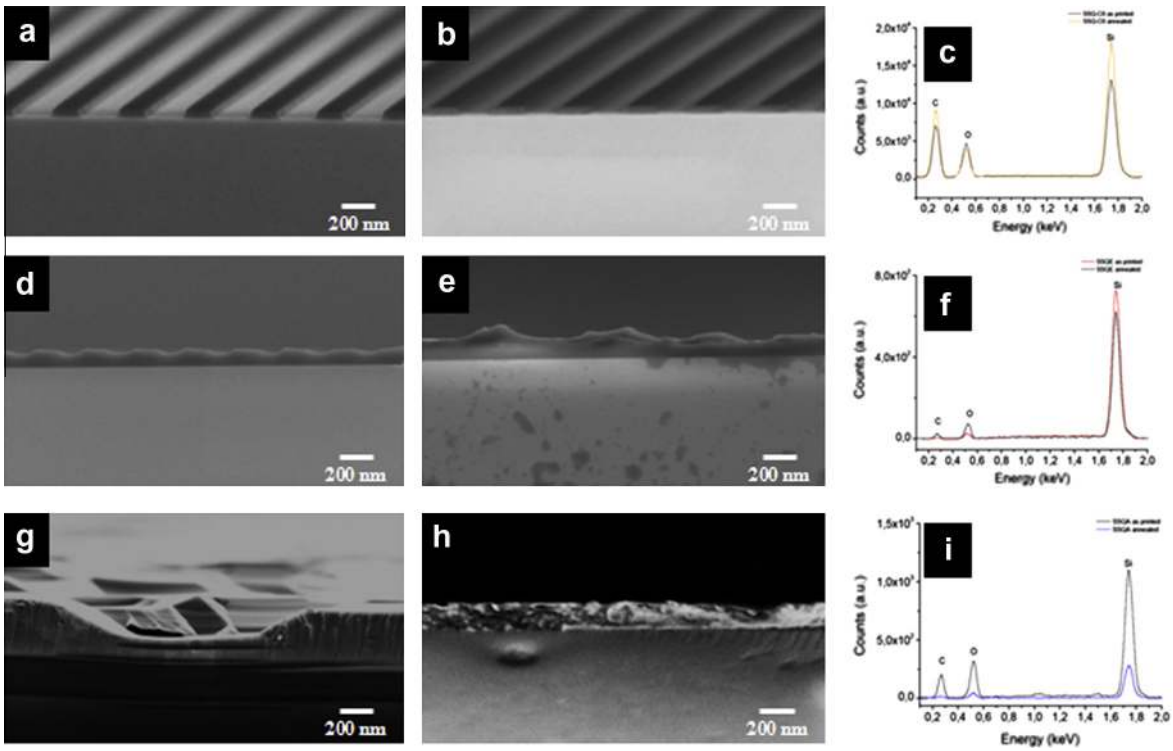

Fig. 5. Patterned POSS substrates behavior under solvent annealing conditions: SEM images of POSS-C6, POSS-epoxy and POSS-acrylo before and after annealing, respectively, (a and b), (d and e) and (g and h). EDX spectra related to the samples POSS-C6 (c), POSS-epoxy (f) and POSS-acrylo (i).

(ellipsometery determined thickness ~4.3 nm and water contact angle 112.4°) facilitates self-assembly in PS-*b*-PDMS with a wetting PDMS layer on the surface and bottom of the film as reported by Ross and Jung [27]. This is due to the PDMS block having considerable lower surface energy than PS and preferentially segregating to the air [32]. The PDMS and PS surface tensions are γ = 19.9 and 40.7 mN m^{-1} repectively [33]. At the substrate-BCP interface, formation of a PDMS wetting layer is expected because of the favorable PDMS block-brush interactions. This 'sandwich' ordains a parallel (to the surface plane) cylinder arrangement. Fig. 2(a) and (b) shows the results of the pre-etch formed oxidized PDMS cylinders obtained from the microphase separated PS-*b*-PDMS films deposited on the PDMS brush. The oxidation of the PDMS cylinders is confirmed with the detection of a Si-O-Si signal at 1098 cm^{-1} (*spectrum omitted for the sake of brevity*). The structure and sequential etching steps are schematically shown in Fig. 2(d) where the PDMS cylinders in a PS matrix are buried underneath a wetting PDMS layer. It is evident that good ordering and correlation length of PDMS cylinders are observed on a macroscopic scale (in microns). The mean PDMS domain spacing, L_0, and line width, <d>, are found to be 42.6 and 23.7 nm respectively. Dewetting and other film effects of PS-*b*-PDMS on the brush remain an issue and as shown in Fig. 2(c), the coverage is poor at around about ~40% of the surface as estimated from SEM. The oval/round shaped areas in Fig. 2(c) are the dewetted regions consisting of single monolayer and multilayer structures.

3.4. Effect of POSS type on BCP self-assembly

The self-assembly of the PS-*b*-PDMS was examined on planar (pre-nanoimprint) POSSs substrates and the results are presented in Fig. 3. The wetting of the surface improved significantly (relative to the PDMS-OH brush) to ~90% coverage with a uniform film thickness. The low magnification SEM image in Fig. 3(d) for POSS-C6 is the direct evidence of superior BCP coverage. The coverage and dewetting issue is similar in POSS-epoxy and POSS-acrylo. There is a major advantage in using POSS modified substrates because the PDMS-OH brush preparation is exacting. It can be seen from the figure that the *in-plane* PDMS cylinders have longer correlation length on POSS-C6 (~3 μm) (Fig. 3(a)) compared to POSS-epoxy (~0.75 μm) (Fig. 3(b)) and POSS-acrylo (~0.40 μm) (Fig. 3(c)). The more disordered structures observed in POSS-epoxy and POSS-acrylo derivatives could be the result of stronger interactions between the minority PDMS block and the POSS layer leading to decreased mass transport and ordering.

3.5. Effect of POSS type on BCP directed self-assembly

The directed self-assembly of PS-*b*-PDMS on topographical POSS substrates was examined. In SEM images (Fig. 4), it is clear the existence of two kinds of self-assembly depending on the POSS derivative. In POSS-C6, the PS-*b*-PDMS system formed PDMS cylinder structures with the cylinders parallel to the surface and along the trenches (Fig. 4(a)). In contrast, in POSS-epoxy and POSS-acrylo

Table 4
EDX analysis of C/Si ratio in as-printed and solvent annealed POSS samples.

POSS type	C/Si ratio	
	As printed	Annealed
POSS-epoxy	0.01	0.08
POSS-acrylo	0.06	0.19
POSS-C6	0.53	0.51

derivatives, the cylinders are parallel to the surface but largely perpendicular to the trenches (Fig. 4(b) and (c)) suggesting that the topography side walls are essentially neutral to both blocks. Unlike the BCP film on PDMS-OH brush with strong dewetting (Fig. 2(c)), the coverage is excellent in POSS coated surfaces as is evident from the low magnification SEM image presented in Fig. 4(d). A schematic presenting the orientation of features in the POSS patterns is outlined in Fig. 4(e).

The neutrality does not appear to be explained by the different hydrophobicity of the POSS modified substrates since POSS-C6 is the most hydrophobic of the materials. It is not so hydrophobic, however, that it favors PDMS cylinders at the sidewalls. However, for the more hydrophilic substrates, it is suggested that the 'neutrality' is not due to solvent parameter type or wetting effects, instead it is due to the interaction of the siloxane groups with labile POSS groups. EDX measurements (Fig. 5) of the films support this hypothesis. The carbon/silicon peak area ratio is very much reduced for POSS-epoxy and POSS-acrylo compared to that seen for POSS-C6 (Fig. 5, Table 4) suggesting loss of organic component. It is also worth noting that substantial degradation of the POSS-epoxy and POSS-acrylo is seen when they are directly (no BCP) exposed to toluene. This suggests that they are extensively swollen by the solvent whilst the POSS-C6 is more resistant because of its' higher hydrophobicity.

4. Conclusions

POSS materials have been shown to be useful materials for producing topographical structures towards directing the self-assembly of a PS-*b*-PDMS BCP. One of the advantages of these systems is that they can be functionalized to engineer their surface chemistry so that BCP wetting and also pattern orientation/alignment can be controlled. The systems should improve wetting compared to conventional polymer brushes that have been used. It was shown that when topographically patterned substrates are used in this way, their ability to direct and control pattern alignment is not predictable from simple concepts such as hydrophobicity and the reactivity of these systems needs to be properly considered. Nanoimprint methodology was shown to be a simple and effective method to topographically pattern these POSSs and produced structures capable of providing excellent pattern alignment to the substrate features. However, the POSSs could be sensitive to the conditions used for solvent annealing the BCP to generate the microphase separated structure. Indeed POSSs can swell and lead to some dissolution effects when exposed to solvent and result in significant damage to the topography. The extent of damage is limited by the presence of the BCP. With solvent annealing becoming a potentially important technique in industrial application of BCP self-assembly methodology, the role of solvent exposure in this type of 'soft graphoepitaxy' has to be very carefully considered.

Associated content

Supporting Information Available

FTIR, ^{1}H NMR and ^{13}C NMR data of synthesized POSS-C6; and FTIR data of oxidized PDMS cylinders after sequential CF_4 and O_2 etches. This material is available free of charge *via* the Internet.

Acknowledgements

Financial support for this work is provided by the EU FP7 NMP project, LAMAND (grant number 245565) project, the Science Foundation Ireland, CRANN CSET grant, and the Spanish MICINN under the project TAPHOR (grant number MAT2012-31392) are gratefully acknowledged.

References

[1] Wissen M, Bogdanski N, Moellenbeck S, Scheer HC. In strategies for hybrid techniques of UV lithography and thermal nanoimprint; 2008.
[2] Chung S, Felts JR, Wang D, King WP, De Yoreo JJ. Temperature-dependence of ink transport during thermal dip-pen nanolithography. Appl Phys Lett 2011;99:193101–3.
[3] Grigorescu AE, Hagen CW. ZResists for sub-20-nm electron beam lithography with a focus on HSQ: state of the art. Nanotechnology 2009;20:292001–31.
[4] Namatsu H, Watanabe Y, Yamazaki K, Yamaguchi T, Nagase M, Ono Y, et al. Fabrication of Si single-electron transistors with precise dimensions by electron-beam nanolithography. J Vac Sci Technol B 2003;21:1–5.
[5] Hirai Y, Hafizovic S, Matsuzuka N, Korvink JG, Tabata O. Validation of X-ray lithography and development simulation system for moving mask deep X-ray lithography. J Microelectromech S 2006;15: 159–68.
[6] Hamley IW. Nanotechnology with soft materials. Angew Chem Int Edit 2003;42:1692–712.
[7] Kumar P. Directed self-assembly: expectations and achievements. Nanoscale Res Lett 2010;5:1367–76.
[8] Ariga K, Hill JP, Lee MV, Vinu A, Charvet R, Acharya S. Challenges and breakthroughs in recent research on self-assembly. Sci Technol Adv Mater 2008;9:014109.
[9] Hawker CJ, Russell TP. Block copolymer lithography: merging "bottom-up" with "top-down" processes. MRS Bull 2005;30:952–66.
[10] Guo LJ. Nanoimprint lithography: methods and material requirements. Adv Mater 2007;19:495–513.
[11] Gates BD, Xu Q, Stewart M, Ryan D, Willson CG, Whitesides GM. New approaches to nanofabrication: molding, printing, and other techniques. Chem Rev 2005;105:1171–96.
[12] Mårtensson T, Carlberg P, Borgström M, Montelius L, Seifert W, Samuelson L. Nanowire arrays defined by nanoimprint lithography. Nano Lett 2004;4:699–702.
[13] Austin MD, Ge H, Wu W, Li M, Yu Z, Wasserman D, et al. Fabrication of 5 nm linewidth and 14 nm pitch features by nanoimprint lithography. Appl Phys Lett 2004;84:5299–301.
[14] Li H-W, Huck WTS. Ordered block-copolymer assembly using nanoimprint lithography. Nano Lett 2004;4:1633–6.

[15] Borah D, Shaw MT, Rasappa S, Farrell RA, O'Mahony CT, Faulkner CM, et al. Plasma etch technologies for the development of ultra-small feature size transistor devices. J Phys D Appl Phys 2011;44:174012–24.
[16] Farrell RA, Kehagias N, Shaw MT, Reboud V, Zelsmann M, Holmes JD, et al. Surface-directed dewetting of a block copolymer for fabricating highly uniform nanostructured microdroplets and concentric nanorings. ACS Nano 2011;5:1073–85.
[17] Salaün M, Kehagias N, Salhi B, Baron T, Boussey J, Sotomayor Torres CM, et al. Direct top-down ordering of diblock copolymers through nanoimprint lithography. J Vac Sci Technol B 2011;29:06F208-12.
[18] Kim TH, Hwang J, Acharya H, Park C. Ordered nanostructure of PS-*b*-PEO copolymer by solvent annealing with mixture of benzene/water vapor and its micropattern fabrication. J Nanosci Nanotechnol 2010;10:6883–7.
[19] Vayer M, Hillmyer MA, Dirany M, Thevenin G, Erre R, Sinturel C. Perpendicular orientation of cylindrical domains upon solvent annealing thin films of polystyrene-b-polylactide. Thin Solid Films 2010;518:3710–5.
[20] Park SM, Liang X, Harteneck BD, Pick TE, Hiroshiba N, Wu Y, et al. Sub-10 nm nanofabrication via nanoimprint directed self-assembly of block copolymers. ACS Nano 2011;5:8523–31.
[21] Politakos N, Ntoukas E, Avgeropoulos A, Krikorian V, Pate BD, Thomas EL, et al. Strongly segregated cubic microdomain morphology consistent with the double gyroid phase in high molecular weight diblock copolymers of polystyrene and poly(dimethylsiloxane). J Poly Sci Part B Polym Phys 2009;47:2419–27.
[22] Borah D, Shaw MT, Holmes JD, Morris MA. Sub-10 nm feature size PS-*b*-PDMS block copolymer structures fabricated by a microwave assisted solvothermal process. ACS Appl Mater Interfaces 2013;5:2004–12.
[23] Borah D, Rasappa S, Senthamaraikannan R, Kosmala B, Shaw MT, Holmes JD, et al. Orientation and alignment control of microphase separated PS-*b*-PDMS substrate patterns *via* polymer brush chemistry. ACS Appl Mater Interfaces 2013;5:88–97.
[24] Cheng JY, Ross CA, Smith HI, Thomas EL. Templated self-assembly of block copolymers: top-down helps bottom-up. Adv Mater 2006;18: 2505–21.
[25] Stoykovich MP, Müller M, Kim SO, Solak HH, Edwards EW, De Pablo JJ, et al. Materials science: directed assembly of block copolymer blends into nonregular device-oriented structures. Science 2005;308:1442–6.
[26] Kim SO, Solak HH, Stoykovich MP, Ferrier NJ, De Pablo JJ, Nealey PF. Epitaxial self-assembly of block copolymers on lithographically defined nanopatterned substrates. Nature 2003;424:411–4.
[27] Jung YS, Ross CA. Orientation-controlled self-assembled nanolithography using a polystyrene-polydimethylsiloxane block copolymer. Nano Lett 2007;7:2046–50.
[28] Zenkiewicz M. Comparative study on the surface free energy of a solid calculated by different methods. Polym Test 2007;26:14–9.
[29] Crivello JV, Malik R. Synthesis and photoinitiated cationic polymerization of monomers with the silsesquioxane core. J Polym Sci Pol Chem 1997;35:407–25.
[30] Son JG, Chang J-B, Berggren KK, Ross CA. Assembly of sub-10-nm block copolymer patterns with mixed morphology and period using electron irradiation and solvent annealing. Nano Lett 2011;11: 5079–84.
[31] Chao CC, Wang T-C, Ho R-M, Georgopanos P, Avgeropoulos A, Thomas EL. Robust block copolymer mask for nanopatterning polymer films. ACS Nano 2010;4:2088–94.
[32] Andersen TH, Tougaard S, Larsen NB, Almdal K, Johannsen I. Surface morphology of PS-PDMS diblock copolymer films. J Electron Spectrosc Relat Phenom 2001;121:93–110.
[33] Chan CM. polymer surface modification and characterization. 1st ed. Munich: Hanser Publishers; 1994.